Nodal gap structure in Fe-based superconductors due to the competition between orbital and spin fluctuations

Tetsuro Saito,[1] Seiichiro Onari,[2] and Hiroshi Kontani[1]
[1]*Department of Physics, Nagoya University, Furo-cho, Nagoya 464-8602, Japan*
[2]*Department of Applied Physics, Nagoya University, Furo-cho, Nagoya 464-8602, Japan*
(Received 22 March 2013; revised manuscript received 24 June 2013; published 11 July 2013)

To understand the origin of the nodal gap structure realized in $BaFe_2(As,P)_2$, we study the three-dimensional gap structure based on the three-dimensional ten-orbital Hubbard model with quadrupole interaction. In this model, strong spin and orbital fluctuations develop when the random-phase approximation is used. By solving the Eliashberg gap equation, we obtain the fully gapped s-wave state with (without) sign reversal between holelike and electronlike Fermi surfaces due to strong spin (orbital) fluctuations, the so-called $s_{\pm}$-wave (s_{++}-wave) state. When both spin and orbital fluctuations develop strongly, which will be realized near the orthorhombic phase, we obtain a nodal s-wave state in the crossover region between the s_{++}-wave and $s_{\pm}$-wave states. The nodal s-wave state obtained possesses loop-shaped nodes on electronlike Fermi surfaces, due to the competition between attractive and repulsive interactions in $\boldsymbol{k}$ space. In contrast, the superconducting gaps on the holelike Fermi surfaces are fully gapped due to orbital fluctuations. The present study explains the main characteristics of the anisotropic gap structure in $BaFe_2(As,P)_2$ observed experimentally.

DOI: 10.1103/PhysRevB.88.045115 PACS number(s): 74.20.−z, 74.20.Fg, 74.20.Rp

I. INTRODUCTION

Since the discovery of Fe-based high-T_c superconductors by Kamihara *et al.*,[1] their many-body electronic properties have been studied very intensively. Figure 1 shows a typical phase diagram of Fe-based superconductors. In the underdoped regime, the second-order orthorhombic (O) structural transition occurs at T_S, and stripe-type magnetic order is realized at $T_N \lesssim T_S$. In the O phase, the orbital polarization $n_{xz} \neq n_{yz}$ is realized, where $n_{xz(yz)}$ is the filling of the $d_{xz(yz)}$ orbital.[2] Also, the softening of the shear modulus C_{66} (Refs. 3–5) and the renormalization of the phonon velocity[6] indicate the development of orbital fluctuations near the orthorhombic phase. Strong spin fluctuations are also observed near the magnetically ordered phase.

These main characteristics of the phase diagram should be understood in order to clarify the mechanism of superconductivity. Theoretical studies of orbital polarization were proposed in Refs. 7–9. However, the *nonmagnetic* structural transition cannot be explained based on the Hubbard model, once we apply the mean-field approximation or the random-phase approximation (RPA). To solve this problem, we recently improved the RPA by including a vertex correction (VC) for the susceptibility that is dropped in the RPA:[10] By applying this self-consistent VC method to the Hubbard model for Fe-based superconductors, both spin and orbital fluctuations mutually develop, and both the O structure transition and the softening of C_{66} can be explained. Note that the "electronic nematic state" with large in-plane anisotropy of resistivity or magnetization well above T_S (Refs. 11–13) also indicates the occurrence of the (local) orbital order.[14]

The phase diagram in Fig. 1 indicates that both spin and orbital fluctuations could be closely related to the mechanism of high-T_c superconductivity. Up to now, the spin-fluctuation-mediated $s_{\pm}$-wave state[15–18] and orbital-fluctuation-mediated s_{++}-wave state[19,20] have been studied based on multiorbital models. The $s_{\pm}$-wave state has a sign reversal of the gap between holelike (h-FSs) and electronlike (e-FSs) Fermi surfaces, whereas the s_{++}-wave state has no sign reversal. Experimentally, the robustness of T_c against impurities in many Fe-based superconductors[21–24] indicates the realization of the s_{++}-wave state, at least in "dirty" compounds with high residual resistivity.[25] Also, the "resonancelike" hump structure in neutron inelastic scattering[26] can be explained by considering the energy dependence of the inelastic scattering if the s_{++}-wave state is realized.

Although a fully gapped s-wave state is realized in many optimally doped high-T_c compounds, a nodal s-wave state (the accidental node is not protected by symmetry) is also observed in some compounds with lower T_c.[27] The appearance of the accidental node strongly indicates the presence of "competing pairing interactions."[28] In the spin fluctuation scenario, if the xy-orbital hole pocket is under the Fermi level, spin fluctuations in the $xz + yz$ orbitals develop at $\boldsymbol{Q} = (\pi,0)$ while those in the xy orbital develop at $\boldsymbol{Q}' = (\pi,\pi/2)$, and this frustration gives a nodal gap structure around the xy-orbital part of the e-FS.[29] This mechanism was studied in detail in Ref. 30 by introducing a phenomenological pairing interaction. However, the xy-orbital h-FS is present in real compounds. In this case, a fully gapped $s_{\pm}$-wave state is obtained by the RPA since spin fluctuations develop at $\boldsymbol{Q} = (\pi,0)$ in all d orbitals, consistently with neutron experiments.[31]

Very interestingly, in optimally doped $BaFe_2(As,P)_2$, a nodal gap structure with high T_c (∼30 K) is realized. The superconducting (SC) gaps on the three h-FSs are fully gapped and almost orbital independent both in the $k_z = \pi$ plane[32] and in the $k_z = 0$ plane,[33] consistently with the orbital fluctuation scenario in Ref. 20. Also, loop-shaped nodes on the e-FSs are observed by angle-resolved thermal conductivity measurements in the vortex state[34] and ARPES measurements.[32,33] These results indicate the existence of competing pairing interactions, and the study of these facts would be significant for understanding the mechanism of high-T_c superconductivity.

On the other hand, the ARPES measurement in Ref. 35 reported the horizontal node on the z^2-orbital e-FS around the

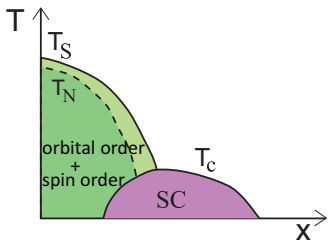

FIG. 1. (Color online) A typical phase diagram for Fe-based superconductors. T_S is the structure transition temperature, which is expected to be induced by orbital polarization $n_{xz} > n_{yz}$ according to angle-resolved photoemission spectroscopy (ARPES) measurements and the sizable softening of C_{66}. T_N is the magnetic transition temperature.

Z point in $BaFe_2(As,P)_2$, contrary to the reports in Refs. 32 and 33. This result is consistent with the prediction of the theory of the spin-fluctuation-mediated $s_\pm$-wave state in Ref. 36. However, the existence of the horizontal node would be inconsistent with the large in-plane field angle dependence of the thermal conductivity reported in Ref. 34. Also, a very small T-linear term in the specific heat in the SC state would not be compatible with the presence of nodes on heavy-hole-like FSs.[37,38]

In this paper, we theoretically study the origin of the nodal gap structure in $BaFe_2(As,P)_2$, in order to obtain significant information about the pairing mechanism of Fe-based superconductors. For this purpose, we construct a three-dimensional (3D) ten-orbital tight-binding model for $BaFe_2(As,P)_2$, and calculate the dynamical spin and orbital susceptibilities due to the combination of Coulomb and quadrupole interactions. By solving the Eliashberg gap equation, we obtain a fully gapped $s_\pm$-wave (s_{++}-wave) state due to strong spin (orbital) fluctuations. When both spin and orbital fluctuations develop strongly, which will be realized near the O phase, a nodal s-wave state with loop-shaped nodes on the e-FSs is realized due to the competition between attractive and repulsive interactions. It is realized during a smooth crossover between s_{++}- and $s_\pm$-wave states.[19,39] In contrast, the SC gaps on the h-FSs are fully gapped due to orbital fluctuations. Thus, the present study explains the main characteristics of the gap structure in $BaFe_2(As,P)_2$.

In Refs. 19, 20, and 40–42 the present authors have shown that the small quadrupole interaction induced by Fe-ion oscillations gives rise to large antiferro- and ferro orbital fluctuations. In addition, we developed the $spin + orbital$ fluctuation theory in the multiorbital Hubbard model by including the VCs to the susceptibilities, which are neglected in the RPA.[10] It was found that the Aslamazov-Larkin-type VC due to Coulomb interaction produces a large effective quadrupole interaction. The emergence of orbital fluctuations due to the VC is also recognized in a simple two-orbital model, using the self-consistent VC method[43] as well as the recently developed two-dimensional renormalization group method.[44]

In Sec. II, we introduce the three-dimensional ten-orbital tight-binding model, which contains two Fe sites in each unit cell. We analyze this model based on the RPA, by taking both the Coulomb and quadrupole interactions into account. The latter interaction originates from the Coulomb interaction beyond the RPA, described by the vertex corrections. In Sec. III, we analyze the SC gap equation for various model parameters, and derive the loop-shaped nodes on the e-FSs due to the competition between orbital and spin fluctuations. Some discussion and a summary are presented in Secs. IV and V, respectively. In Appendix A, we show the obtained orbital fluctuations that give the s_{++}-wave state with nearly isotropic gap functions on the three h-FSs. In Appendix B, we discuss the SC state in heavily electron-doped systems when the xy-orbital h-FS disappears.

II. FORMULATION

In this paper, we set the x and y axes parallel to the nearest Fe-Fe bonds, and the orbitals z^2, xz, yz, xy, and x^2-y^2 are denoted as 1, 2, 3, 4, and 5, respectively. First, we perform a local-density-approximation (LDA) band calculation for $BaFe_2As_2$ and $BaFe_2P_2$ using the WIEN2K code based on the known crystal structure. Next, we derive a ten-orbital tight-binding model that reproduces the LDA band structure and its orbital character using the WANNIER90 code and the WIEN2WANNIER interface.[45] Using the two sets of tight-binding parameters obtained (hopping integrals and on-site energies), the parameters of $BaFe_2(As_{1-x}P_x)_2$ are well approximated by making a linear combination of them with a ratio of $(1-x):x$.[36] In this paper, we use the tight-binding parameters for $x = 0.30$. The kinetic term obtained is given as

$$\hat{H}^0 = \sum_{ab\alpha\beta lm\sigma} t_{lm}^{a\alpha,b\beta} c_{la\alpha,\sigma}^\dagger c_{mb\beta,\sigma} = \sum_{ab\alpha\beta lm\sigma} \sum_{\boldsymbol{k}} t_{lm}^{a\alpha,b\beta} e^{i\boldsymbol{k}\cdot(\boldsymbol{R}_{a,\alpha}-\boldsymbol{R}_{b,\beta})} c_{l\alpha,\sigma}^\dagger(\boldsymbol{k}) c_{m\beta,\sigma}(\boldsymbol{k}), \quad (1)$$

where a,b represent the unit cell, α,β ($= A, B$) represent the two Fe sites, l,m = 1–5 represent the d orbital, and $\sigma = \pm 1$ is the spin index. $\boldsymbol{R}_{a,\alpha}$ is the position of the Fe site, $c_{la\alpha,\sigma}^\dagger$ is the creation operator of the d electron, and $t_{lm}^{a\alpha,b\beta}$ with $a = b$ and $\alpha = \beta$ ($a \neq b$ or $\alpha \neq \beta$) is the local potential (hopping integral).

However, the xy-orbital h-FS given by the LDA is too small compared to the experimental results from ARPES measurements. In order to increase the size of the xy-orbital h-FS, we introduce the following orbital-dependent potential term around the Γ point:

$$\hat{H}^{\rm kin} = \hat{H}^0 + \sum_{l\alpha,\sigma} \sum_{\boldsymbol{k}} e_l \left[\frac{\cos k_x \cos k_y + 1}{2}\right] c_{l\alpha,\sigma}^\dagger(\boldsymbol{k}) c_{l\alpha,\sigma}(\boldsymbol{k}), \quad (2)$$

where e_l is the energy shift of the orbital l at the Γ point. We put $e_{xy} = 0.02$ eV, $e_{xz} = e_{yz} = -0.01$ eV, and the others are 0. The FSs in this model are composed of three h-FSs around the Γ point and four e-FSs around the X and Y points. Figure 2 shows the FSs obtained in the (a) $k_z = 0$ and (b) $k_y = 0$ planes, respectively. The electron filling per Fe site is $n = 6.0$. In Fig. 2(b), there are three h-FSs (FS1, FS2, and FS3) and two e-FSs (FS4 and FS5). We call FS4 (FS5) the outer (inner) e-FS.

Next, we explain the interaction term. We introduce both the Coulomb interaction (U, U', $J = (U-U')/2$) and

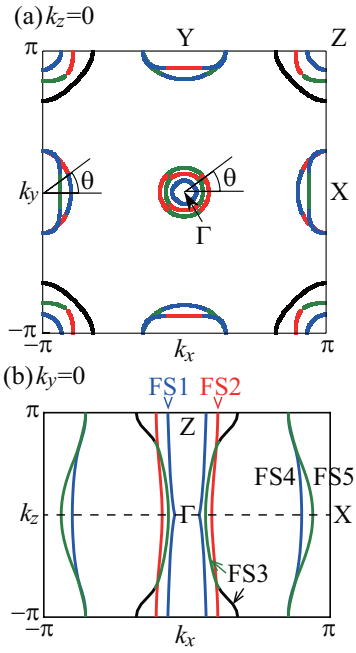

FIG. 2. (Color online) The Fermi surfaces in the (a) $k_z = 0$ plane and (b) $k_y = 0$ plane of the present ten-orbital model for the filling $n = 6.0$. The green, red, blue, and black lines correspond to the xz, yz, xy, and z^2 orbitals, respectively. In (b), there are three h-FSs (FS1, FS2, and FS3) and four e-FSs (FS4 and FS5).

the quadrupole interactions. The latter are induced by the electron-phonon (e-ph) interaction due to Fe ion oscillations as follows:[41]

$$V_{\rm quad} = -g_1(\omega_l)\sum_i^{\rm site}\left(\hat{O}^i_{yz}\cdot\hat{O}^i_{yz}+\hat{O}^i_{xz}\cdot\hat{O}^i_{xz}\right) - g_2(\omega_l)\sum_i^{\rm site}\left(\hat{O}^i_{xy}\cdot\hat{O}^i_{xy}\right), \quad (3)$$

where $g_i(\omega_l) = g_i\omega_D^2/(\omega_l^2+\omega_D^2)$, and $g_i = g_i(0)$ is the quadrupole interaction at $\omega_n = 0$. ω_D is the cutoff energy of the quadrupole interaction. $\hat{O}_\Gamma$ is the quadrupole operator introduced in Ref. 19, which will be shown in Appendix A. $\hat{V}_{\rm quad}$ has many nonzero off-diagonal elements as explained in Ref. 19. As also explained in Ref. 19, g_1 (g_2) is induced by in-plane (out-of-plane) Fe-ion oscillations. In this paper, we put $g_1 = g_2 = g$ unless otherwise noted. Also, the Aslamazov-Larkin-type VC due to the Coulomb interaction produces a large effective quadrupole interaction g_1.[10] Thus, the quadrupole interaction in Eq. (3) is derived from both the VC and the e-ph interaction.

Now, we perform the RPA for the present model, by using $32\times32\times16$ $\boldsymbol{k}$ meshes. The irreducible susceptibility in the ten-orbital model is given by

$$\chi^{(0)\alpha\beta}_{ll',mm'}(q) = -\frac{T}{N}\sum_k G^{\alpha\beta}_{lm}(k+q)\,G^{\beta\alpha}_{m'l'}(k), \quad (4)$$

where $q = (\boldsymbol{q},\omega_l)$ and $k = (\boldsymbol{k},\epsilon_n)$. $\epsilon_n = (2n+1)\pi T$ and $\omega_l = 2l\pi T$ are the fermion and boson Matsubara frequencies. $\hat{G}(k) = [i\epsilon_n + \mu - \hat{h}^{\rm kin}_{\boldsymbol{k}}]^{-1}$ is the d-electron Green function in the orbital basis, where $\hat{h}^{\rm kin}_{\boldsymbol{k}}$ are the matrix elements of $\hat{H}^{\rm kin}$ and μ is the chemical potential. Then, the susceptibilities for the spin and charge sectors in the RPA are given by[46]

$$\hat{\chi}^s(q) = \frac{\hat{\chi}^{(0)}(q)}{\hat{1}-\hat{\Gamma}^s\hat{\chi}^{(0)}(q)}, \quad (5)$$

$$\hat{\chi}^c(q) = \frac{\hat{\chi}^{(0)}(q)}{\hat{1}-\hat{\Gamma}^c(\omega_l)\hat{\chi}^{(0)}(q)}, \quad (6)$$

where

$$(\Gamma^s)^{\alpha\beta}_{l_1l_2,l_3l_4} = \delta_{\alpha,\beta}\times\begin{cases}U, & l_1=l_2=l_3=l_4,\\ U', & l_1=l_3\neq l_2=l_4,\\ J, & l_1=l_2\neq l_3=l_4,\\ J', & l_1=l_4\neq l_2=l_3,\\ 0 & \text{otherwise},\end{cases} \quad (7)$$

$$\hat{\Gamma}^c(\omega_l) = -\hat{C} - 2\hat{V}_{\rm quad}(\omega_l), \quad (8)$$

$$(C)^{\alpha\beta}_{l_1l_2,l_3l_4} = \delta_{\alpha,\beta}\times\begin{cases}U, & l_1=l_2=l_3=l_4,\\ -U'+2J, & l_1=l_3\neq l_2=l_4,\\ 2U'-J, & l_1=l_2\neq l_3=l_4,\\ J', & l_1=l_4\neq l_2=l_3,\\ 0 & \text{otherwise},\end{cases} \quad (9)$$

where $\alpha,\beta = A,B$.

In the RPA, the enhancement of the spin susceptibility $\hat{\chi}^s$ is mainly caused by the intraorbital Coulomb interaction U, using the "intraorbital nesting" of the FSs. On the other hand, the enhancement of $\hat{\chi}^c$ in the present model is caused by the quadrupole-quadrupole interaction in Eq. (3), utilizing the "interorbital nesting" of the FSs. The magnetic (orbital) order is realized when the spin (charge) Stoner factor $\alpha_{s(c)}$, which is the maximum eigenvalue of $\hat{\Gamma}^{s(c)}\hat{\chi}^{(0)}(\boldsymbol{q},0)$, is unity. When $n = 6.0$, the critical value of U is $U_{\rm cr} = 1.18$ eV, and the critical value of g is $g_{\rm cr} = 0.23$ eV for $U = 0$. Hereafter, we set the unit of energy as eV.

Next, we explain the linearized Eliashberg equation. In order to obtain the fine momentum dependence of the SC gap, we concentrate on the gap functions only on the FSs as was done in Ref. 29: We used 40×16 $\boldsymbol{k}$ points for each Fermi surface sheet. In the presence of dilute impurities ($n_{\rm imp} \ll 1$), the linearized Eliashberg equation is given as[29]

$$Z^i(\boldsymbol{k},\epsilon_n)\lambda_E\Delta^i(\boldsymbol{k},\epsilon_n) = \frac{\pi T}{(2\pi)^3}\sum_{\epsilon_m}\sum_j^{\rm FS}\int_{{\rm FS}j}\frac{d\boldsymbol{k}'_{{\rm FS}j}}{v^j(\boldsymbol{k}')}V^{ij}(\boldsymbol{k},\boldsymbol{k}',\epsilon_n-\epsilon_m) \times\frac{\Delta^j(\boldsymbol{k}',\epsilon_m)}{|\epsilon_m|} + \delta\Sigma^i_{\rm a}(\boldsymbol{k},\epsilon_n), \quad (10)$$

where λ_E is the eigenvalue that reaches unity at $T = T_{\rm c}$. i and j denote the FSs, and $\Delta^i(\boldsymbol{k},\epsilon_n)$ is the gap function on the ith FS (FSi) at the Fermi momentum $\boldsymbol{k}$. The integral in Eq. (10) means the surface integral on FSj. The pairing interaction V in Eq. (10) is

$$V^{ij}(\boldsymbol{k},\boldsymbol{k}',\epsilon_n-\epsilon_m) = \sum_{l_i,\alpha\beta}U^*_{l_1\alpha,i}(\boldsymbol{k})U_{l_4\beta,i}(\boldsymbol{k})V^{\alpha\beta}_{l_1l_2,l_3l_4} \times(\boldsymbol{k}-\boldsymbol{k}',\epsilon_n-\epsilon_m)U_{l_2\alpha,j}(\boldsymbol{k}')U^*_{l_3\beta,j}(\boldsymbol{k}'), \quad (11)$$

$$\hat{V} = \hat{V}^c + \hat{V}^s + \hat{V}^{(0)}, \tag{12}$$

$$\hat{V}^c = \frac{1}{2}\hat{\Gamma}^c \hat{\chi}^c \hat{\Gamma}^c, \quad \hat{V}^s = -\frac{3}{2}\hat{\Gamma}^s \hat{\chi}^s \hat{\Gamma}^s, \tag{13}$$

$$\hat{V}^{(0)} = \frac{1}{2}(\hat{\Gamma}^c - \hat{\Gamma}^s), \tag{14}$$

where $U_{l\alpha,i}(\boldsymbol{k}) = \langle \boldsymbol{k}; l\alpha | \boldsymbol{k}; i \rangle$ is the transformation unitary matrix between the band and the orbital representations.

In Eq. (10), Z is given as

$$Z^i(\boldsymbol{k},\epsilon_n) = 1 + \frac{\gamma^i(\boldsymbol{k},\epsilon_n)}{|\epsilon_n|}, \tag{15}$$

where γ^i is the impurity-induced quasiparticle damping rate. Here, we calculate the damping rate using the T-matrix approximation. We consider the case of Fe-site substitution, where the impurity potential I is diagonal in the d-orbital basis. The T matrix for an impurity at the α ($=A$ or B) site is given as

$$\hat{T}^\alpha(\epsilon_n) = \left[\hat{1} - \hat{I}^\alpha \hat{G}^\alpha_{\rm loc}(\epsilon_n)\right]^{-1} \hat{I}^\alpha, \tag{16}$$

which is $\boldsymbol{k}$ independent in the orbital basis. Here, $I^\alpha_{l,l'} = I\delta_{l,l'}$ is the impurity potential, and $\hat{G}^\alpha_{\rm loc}$ is the local Green function given as

$$[G_{\rm loc}]^\alpha_{ll'}(\epsilon_n) = \frac{1}{N}\sum_{\boldsymbol{k}'} G^\alpha_{ll'}(\boldsymbol{k}',\epsilon_n) = -s_n \frac{i\pi}{(2\pi)^3}\sum_j \int_{{\rm FS}j} \frac{d\boldsymbol{k}'_{{\rm FS}j}}{v^j(\boldsymbol{k}')} U_{l\alpha,j}(\boldsymbol{k}') U^*_{l'\alpha,j}(\boldsymbol{k}'), \tag{17}$$

where $s_n = {\rm sgn}(\epsilon_n)$.

In the T-matrix approximation, which is exact for $n_{\rm imp} \ll 1$, the normal self-energy in the band-diagonal basis is given as

$$\delta\Sigma^i_n(\boldsymbol{k},\epsilon_n) = n_{\rm imp}\sum_{ll'\alpha} U^*_{l\alpha,i}(\boldsymbol{k}) T^\alpha_{ll'}(\epsilon_n) U_{l'\alpha,i}(\boldsymbol{k}), \tag{18}$$

where $n_{\rm imp}$ is the impurity concentration ratio. Then the quasiparticle damping rate is given as

$$\gamma^i(\boldsymbol{k},\epsilon_n) = -{\rm Im}\delta\Sigma^i_n(\boldsymbol{k},\epsilon_n)s_n. \tag{19}$$

Also, $\delta\Sigma^i_a$ is the impurity-induced anomalous self-energy given as

$$\delta\Sigma^i_a(\boldsymbol{k},\epsilon_n) = n_{\rm imp}\sum_{ll'\alpha} U^*_{l\alpha,i}(\boldsymbol{k}) U_{l'\alpha,i}(\boldsymbol{k}) \times \sum_{mm'} T^\alpha_{lm}(\epsilon_n) X^\alpha_{mm'}(\epsilon_n) T^\alpha_{l'm'}(-\epsilon_n), \tag{20}$$

where

$$X^\alpha_{mm'}(i\epsilon_n) = \frac{\pi}{(2\pi)^3}\sum_j \int_{{\rm FS}j} \frac{d\boldsymbol{k}'_{{\rm FS}j}}{v^j(\boldsymbol{k}')} U_{m\alpha,j}(\boldsymbol{k}') \times U^*_{m'\alpha,j}(\boldsymbol{k}') \frac{\Delta^j(\boldsymbol{k}',\epsilon_n)}{|\epsilon_n|}. \tag{21}$$

In this calculation, we simplify the energy dependence of $\hat{V}$. We assume that $\hat{V}^\xi$ ($\xi = c,s$) can be separated into the momentum- and orbital-dependent part $\hat{V}^\xi(\boldsymbol{k},\omega_l = 0)$ and the energy-dependent part $g_\xi(\omega_l)$:

$$\hat{V}^\xi(\boldsymbol{k},\omega_l) = \hat{V}^\xi(\boldsymbol{k},\omega_l = 0) \times g_\xi(\omega_l). \tag{22}$$

We calculated $\hat{V}^\xi(\boldsymbol{k},\omega_l = 0)$ without approximation. On the other hand, $g_\xi(\omega_l)$ is determined approximately as

$$g_\xi(\omega_l) = {\rm Re}\left[\frac{V^\xi_{\rm max}(\omega_l)}{V^\xi_{\rm max}(\omega_l = 0)}\right], \tag{23}$$

where $V^\xi_{\rm max}(0)$ is the largest value of $V^{\xi,\alpha\beta}_{l_1l_2,l_3l_4}(\boldsymbol{k},\omega_l = 0)$ for any α, β, l_i, and $\boldsymbol{k}$. It is verified that this simplification affects the momentum dependence of the SC gap functions only quantitatively, although the λ_E obtained is quantitatively underestimated. Thus, this approximation would be appropriate for the present purpose, that is, the analysis of the anisotropy of the SC gap.

III. SUPERCONDUCTING GAP

In this section, we analyze the linearized Eliashberg equation (10) using the 3D model of $BaFe_2(As,P)_2$ for $n = 6.0$. Hereafter, we use $32 \times 32 \times 16$ $\boldsymbol{k}$ meshes for calculating the charge and spin susceptibilities. We assume that $J = J'$ and $U = U' + 2J$, and fix the ratio $J/U = 1/6$. In solving the Eliashberg equation, we used 40×16 $\mathbf{k}$ points for each Fermi surface sheet and 512 Matsubara frequencies. In this paper, we perform the calculation at $T = 0.005$ and $\omega_D = 0.02$.

A. $s_\pm$-wave SC gap mediated by spin fluctuations

First, we study the spin-fluctuation-mediated $s_\pm$-wave superconducting state for $U \lesssim U_{\rm cr}$ by putting $g = 0$ and $n_{\rm imp} = 0$. Here, we put $U = 1.15$ ($\alpha_s = 0.98$), and the eigenvalue obtained is $\lambda_E = 1.01$. The gap structure obtained is almost independent of α_s. First, we discuss the SC gaps on the h-FSs. Figures 3(a) and 3(b) show the gap functions obtained on the h-FSs in the $k_z = 0$ and π planes, respectively. The definitions of θ and FS1-5 are shown in Fig. 2. In the $k_z = 0$ plane, the SC gap size weakly depends on the orbital character of the FSs. However, in the $k_z = \pi$ plane, the SC gap size strongly depends on the d orbital. In particular, the SC gap on the z^2-orbital FS is almost zero and negative, reflecting the small spin fluctuations in the z^2 orbital because of the absence of intra-z^2-orbital nesting. (Note that the z^2 orbital is absent on the e-FSs.) The horizontal node is clearly recognized in the SC gap in the $k_y = 0$ plane shown in Fig. 3(c). The horizontal node obtained on FS3 near $k_z = \pi$ is consistent with the previous RPA calculation by Suzuki *et al.*[36]

The obtained horizontal node would contradict the fourfold symmetry of the thermal conductivity[34] and the small Volovik effect in the specific heat measurement.[37,38] According to ARPES measurements, the horizontal node was reported in Ref. 35, whereas it was not observed in Refs. 32 and 33.

Next, we discuss the SC gaps on the e-FSs. Figures 3(d) and 3(e) show the gap functions obtained on the e-FSs in the $k_z = 0$ and π planes, respectively. As we can see, line nodes do not appear on the e-FSs. This result is consistent with the analysis in Ref. 31, that is, the $s_\pm$-wave gap on the e-FSs is fully gapped if a h-FS made of xy orbital appears. Note that the SC gaps for $k_z = \pi$ in Fig. 3(e) are obtained by rotating the gaps in the $k_z = 0$ plane in (d) by $\pi/2$. Also, Figs. 3(f)

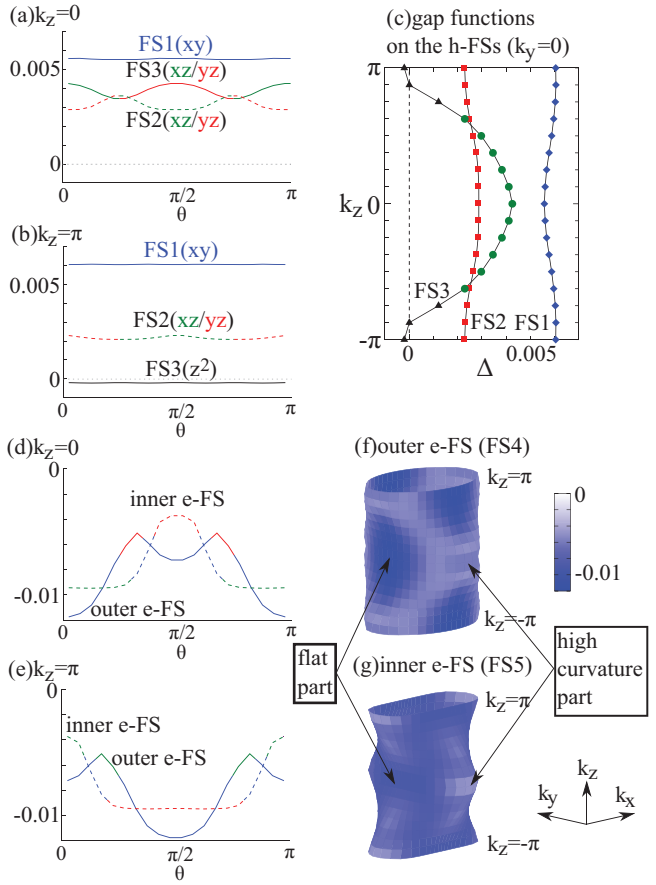

FIG. 3. (Color online) SC gap functions obtained for $U = 1.15$ and $g = 0$. (a), (b) SC gap functions on the h-FSs in the $k_z = 0$ and $k_z = \pi$ planes. The green, red, blue, and black lines correspond to the xz, yz, xy, and z^2 orbitals, respectively. (c) k_z dependence of the SC gaps on the h-FSs in the $k_y = 0$ planes. A horizontal node appears on the FS3 around $k_z = \pm\pi$. (d), (e) SC gap functions on the e-FSs in the $k_z = 0$ and $k_z = \pi$ planes. (f), (g) 3D gap functions on the outer and inner e-FSs.

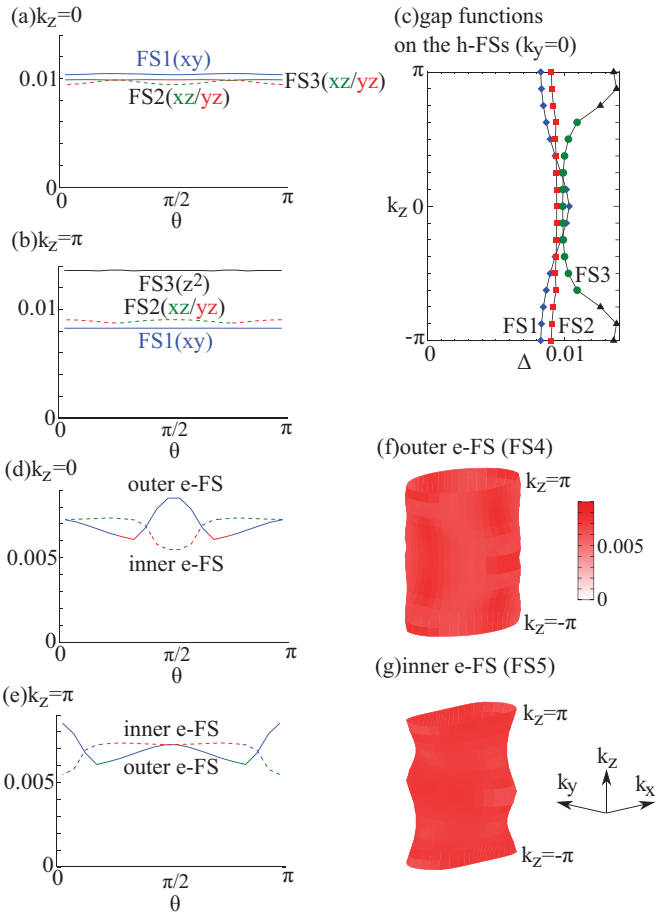

FIG. 4. (Color online) SC gap functions obtained for $g = 0.22$ and $U = 0$. (a), (b) SC gap functions on the h-FSs in the $k_z = 0$ and $k_z = \pi$ planes. The green, red, blue, and black lines correspond to the xz, yz, xy, and z^2 orbitals, respectively. (c) k_z dependence of the SC gaps on the h-FSs in the $k_y = 0$ plane. The colors used are the same as in (a) and (b). (d), (e) SC gap functions on the e-FSs in the $k_z = 0$ and $k_z = \pi$ planes. (f), (g) 3D gap functions on the outer and inner e-FSs.

and 3(g) show 3D gap functions on the outer and inner FSs (FS4 and FS5), respectively. On both e-FSs, the SC gap on the "flat part" is larger than that on the "high-curvature part."

B. s_{++}-wave SC gap mediated by orbital fluctuations

Next, we study the orbital-fluctuation-mediated s_{++}-state superconducting state for $g \lesssim g_{\rm cr}$ by putting $U = 0$ and $n_{\rm imp} = 0$. Here, we put $g = 0.22$ ($\alpha_c = 0.98$), and the eigenvalue obtained is $\lambda_E = 0.59$. The gap structure obtained is almost independent of α_c. Figures 4(a) and 4(b) show the gaps obtained on the h-FSs in the $k_z = 0$ and π planes, respectively. In great contrast to the spin fluctuation scenario, the gap size on the z^2-orbital FS is comparable with that on the other FSs, since strong orbital correlations are developed in all d orbitals: Note that the quadrupole interaction possesses many nonzero interorbital matrix elements. The present numerical result is consistent with our previous calculation using the 2D five-orbital model.[20]

Figure 4(c) shows that the SC gap size of each h-FS is approximately independent of k_z, which is consistent with the small orbital dependence of the SC gap in $(Ba,K)Fe_2As_2$ and $BaFe_2(As,P)_2$ observed in Refs. 32 and 33. Figures 4(d) and 4(e) show the gaps obtained on the e-FSs in the $k_z = 0$ and π planes, respectively. Figures 4(f) and 4(g) show the 3D SC gap functions on the outer and inner e-FSs (FS4 and FS5), respectively. Thus, the SC gap obtained on the e-FSs is isotropic for any k_z.

We also discuss the SC gap functions in the case of $g_1 = g$ and $g_2 = 0$ in Eq. (3). Figure 5 shows the k_z dependence of the SC gaps on the h-FSs for $g = 0.24$ ($\alpha_c = 0.98$) and $U = 0$. In this case, the gap function on the z^2-orbital h-FS is smaller compared to the case of $g_1 = g_2 = g$ in Fig. 4. On the other hand, the SC gaps obtained on the e-FSs are almost isotropic, similarly to the results for $g_1 = g_2 = g$.

C. Loop-shaped node due to the competition of spin and orbital fluctuations

Recently, several measurements observed the nodal gap structure in $BaFe_2(As_{1-x}P_x)_2$.[32–34] This compound is very

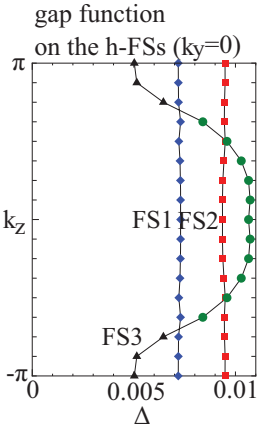

FIG. 5. (Color online) k_z dependence obtained of the SC gaps on the h-FSs in the $k_y = 0$ plane. The parameters used are $g_1 = 0.24$, $g_2 = 0$, and $U = 0$.

clean, and very accurate measurements of the gap structure have been performed. They present a significant challenge for theories in reproducing the observed gap structure. However, as discussed in Secs. III A and III B, we cannot reproduce the line nodes on the electron FSs when either spin or orbital fluctuations develop alone.

Here, we study the emergence of a highly anisotropic s-wave state due to the strong orbital and spin fluctuations. In the phase diagram of $BaFe_2(As_{1-x}P_x)_2$, both T_N and T_S decrease to zero at almost the same critical point $x_c \approx 0.3$. This fact means that both spin and orbital fluctuations become comparable in magnitude at $x \sim x_c$. Here, we consider the case that the s_{++}-wave state is realized by stronger orbital fluctuations. On increasing the spin fluctuation with momentum $\boldsymbol{Q}$, $\Delta_{\boldsymbol{k}}$ and $\Delta_{\boldsymbol{k}+\boldsymbol{Q}}$ are suppressed when both $\boldsymbol{k}$ and $\boldsymbol{k}+\boldsymbol{Q}$ are on FSs with the same orbital character, and finally the sign change $\Delta_{\boldsymbol{k}} \cdot \Delta_{\boldsymbol{k}+\boldsymbol{Q}} < 0$ can be achieved. Such strong anisotropy originates from the competition between the attractive interaction of V^c and the repulsive interaction of V^s in Eq. (13). As shown in Fig. 6, strong spin fluctuations on the xy orbital (due to intra-xy-orbital nesting) produce the loop-shaped node on the e-FS. A similar "anisotropic s-wave gap modified by the spin fluctuations" is considered to be realized in (Y,Lu)Ni_2B_2C.[28]

Hereafter, we present numerical results in the presence of a small amount of impurities ($I = 1$ and $n_{\rm imp} = 0.03$),

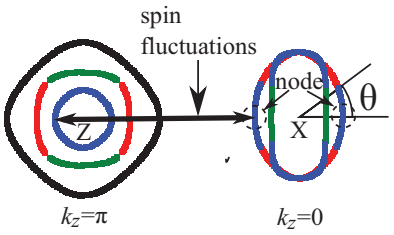

FIG. 6. (Color online) Formation of the nodal s-wave gap (shown in Fig. 7) due to the competition of orbital fluctuations (=interorbital attraction) and spin fluctuations (=intraorbital repulsion). Green, red, blue, and black lines correspond to the xz, yz, xy, and z^2 orbitals, respectively.

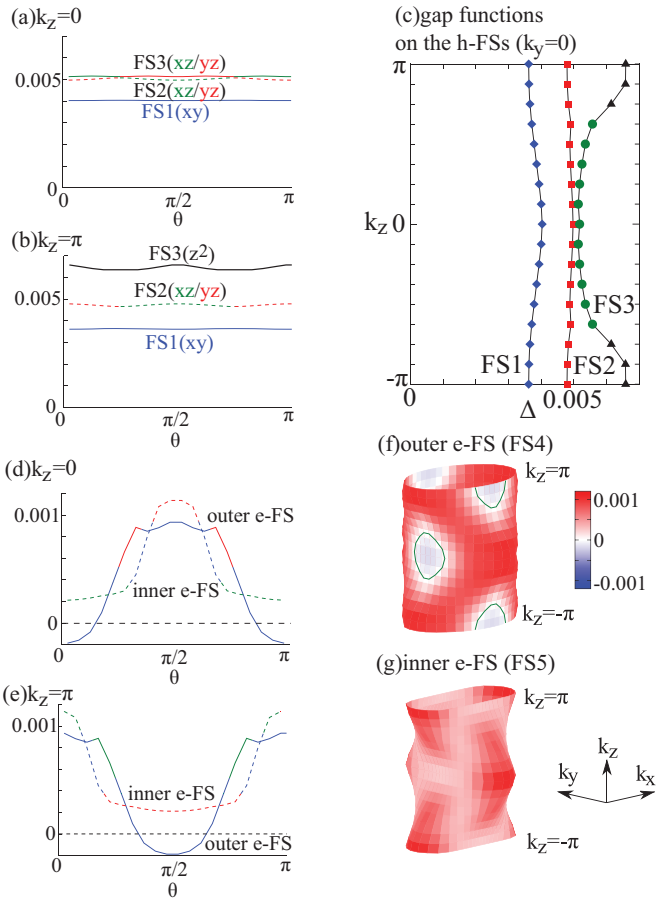

FIG. 7. (Color online) SC gap functions obtained for $g = 0.204$, $U = 1.011$, and $n_{\rm imp} = 0.03$. (a), (b) SC gap functions on the h-FSs in the $k_z = 0$ and $k_z = \pi$ planes. (c) k_z dependence of SC gaps on the hole FSs in the $k_y = 0$ plane. (d), (e) SC gap functions on the e-FSs in the $k_z = 0$ and $k_z = \pi$ planes. (f), (g) 3D gap functions on the outer and inner e-FSs. The green lines represent the gap nodes.

just to make the SC gap functions smoother. Figure 7 shows the results for a nearly s_{++}-wave state with nodal structure on the outer e-FS. We put $g = 0.204$ and $U = 1.011$ ($\alpha_c = 0.980$, $\alpha_s = 0.859$), and the eigenvalue is $\lambda_E = 0.50$. Figures 7(a)–7(c) show the SC gaps obtained on the h-FSs in the $k_z = 0$ plane, $k_z = \pi$ plane, and $k_y = 0$ plane, respectively. The SC gaps obtained on the h-FSs are nearly isotropic and orbital independent, similarly to the results in Fig. 4. In particular, the gap size of the z^2-orbital h-FS is large even in the presence of loop-shaped nodes on the e-FSs.

Figures 7(d) and 7(e) show the SC gaps obtained on the e-FSs in the $k_z = 0$ and π planes, respectively. The SC gap on the inner e-FS is fully opened, and its sign is the same as that on the h-FSs. On the outer e-FS, in contrast, the SC gap shows a sign change near $\theta = 0, \pi$ ($\theta = \pi/2, 3\pi/2$) in the $k_z = 0$ plane ($k_z = \pi$ plane). This sign change is caused by strong spin fluctuations in the xy orbital, as we have explained in Fig. 6. In this case, the SC gaps on the h-FSs remain fully gapped, due to the fact that the band mass of the h-FSs is larger than that of the e-FSs. As a result, closed loop-shaped nodes appear in the flat part on the outer e-FS, as recognized in Figs. 7(f) and 7(g). This gap structure is consistent with the

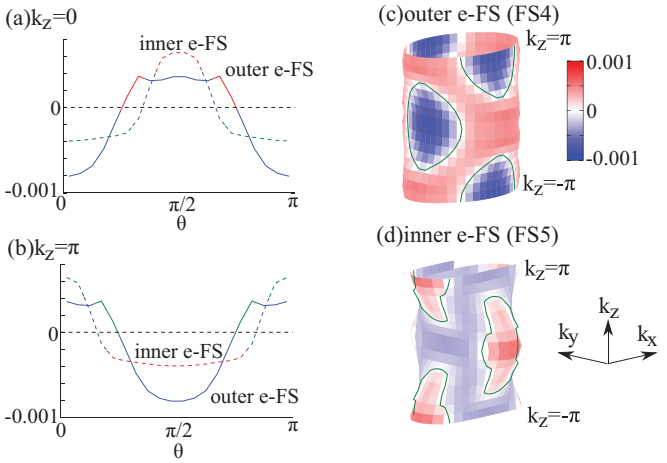

FIG. 8. (Color online) SC gap function obtained for $g = 0.204$ and $U = 1.017$. (a), (b) SC gap functions on the e-FSs in the $k_z = 0$ and $k_z = \pi$ planes. (c), (d) 3D gap functions on the outer and inner e-FSs. The green lines represent the gap nodes.

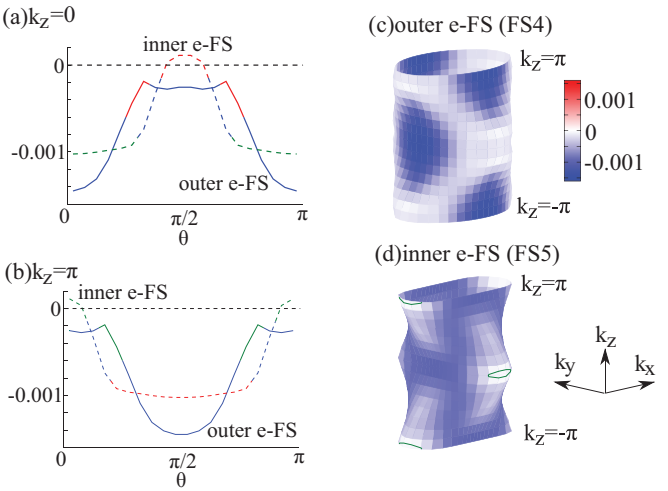

FIG. 9. (Color online) SC gap functions obtained for $g = 0.204$ and $U = 1.023$. (a), (b) SC gap functions in the e-FSs on the $k_z = 0$ and $k_z = \pi$ planes. (c), (d) 3D gap functions on the outer and inner e-FSs. The green lines represent the gap nodes.

prediction given by the angle-resolved thermal conductivity under a magnetic field.[34]

On increasing the value of U (or reducing $n_{\rm imp}$) slightly, the area of the sign-reversed part on the outer e-FS increases, and the SC gap on the inner e-FS also shows the sign reversal. Figures 8(a) and 8(b) show the SC gap functions on the e-FSs for $g = 0.204$ and $U = 1.017$ ($\alpha_c = 0.980$ and $\alpha_s = 0.864$). The eigenvalue obtained is $\lambda_E = 0.50$. The gap functions obtained are approximately given by shifting the gaps in Figs. 7(d) and 7(e) downwards, and line nodes appear on both the inner and outer e-FSs. As described in Figs. 8(c) and 8(d), closed nodal loops appear in the flat part on the outer e-FS and in the high-curvature part on the inner e-FS. The SC gaps on the h-FSs are almost the same as those shown in Figs. 7(a)–7(c), so we do not show them.

On increasing the value of U (or reducing $n_{\rm imp}$) further, the sign of the SC gap on the outer e-FS is completely reversed, and small closed-loop nodes appear only on the inner e-FS. The obtained SC gaps are nearly $s_{\pm}$-wave state. Figures 9(a) and 9(b) show the gap functions obtained on the e-FSs for $g = 0.204$ and $U = 1.023$ ($\alpha_c = 0.980$, $\alpha_s = 0.869$). The eigenvalue obtained is $\lambda_E = 0.50$. They are approximately given by shifting the gaps in Figs. 8(a) and 8(b) downwards. Figures 9(c) and 9(d) show the 3D gap functions obtained on the outer and inner e-FSs, respectively. Apparently, closed nodal loops appear in the high-curvature part on the inner e-FS, whereas no nodes appear on the outer e-FS. This numerical result is consistent with the recent ARPES measurement by Yoshida *et al.*.[33] On the other hand, the SC gaps on the h-FSs are similar to those in Figs. 7(a)–7(c).

In Figs. 7–9, we fixed the impurity parameters as $n_{\rm imp} = 0.03$ and $I = 1$. Now, we discuss the SC gap functions for general impurity parameters. Figure 10(a) shows the U-$n_{\rm imp}$ phase diagram for both $I = 1$ and $I = 0.3$. The solid (dashed) lines represent the boundaries between s_{++} wave and nodal-s wave, or nodal-s wave and $s_{\pm}$ wave for $I = 1$ ($I = 0.3$). On decreasing α_s or increasing α_c, the following crossover would be realized: (i) full gap $s_{\pm}$ wave $\rightarrow$ (ii) nodal s wave $\rightarrow$ (iii) full gap s_{++} wave. When both U and g are fixed, the same crossover occurs when $n_{\rm imp}$ increases. The residual resistivity for $I = 1$ derived from the linear response theory is about 20 $\mu\Omega$ cm per $n_{\rm imp} = 0.01$.

We note that, in the present numerical calculation using a 3D model, line nodes can appear even if $n_{\rm imp} = 0$ as shown in Fig. 10. In contrast, in the previous calculation using the 2D model,[20,42] we could not obtain the line nodes for $n_{\rm imp} = 0$, since the SC state changes from the s_{++} wave to the $s_{\pm}$ wave discontinuously as U increases.

In the present study based on the RPA, the $s_{++} \leftrightarrow s_{\pm}$ crossover is realized in the case of $\alpha_s \ll \alpha_c$ (=0.98) for $n_{\rm imp} \ll 0.1$. One of the main reasons would be the factor 3 in front of V^s in Eq. (13), reflecting the SU(2) symmetry of the spin space. However, this factor 3 might be overestimated since recent polarized neutron scattering measurements indicate the relation $\chi^s_z(\boldsymbol{Q}) \gg \chi^s_{x,y}(\boldsymbol{Q})$ above T_c due to the spin-orbit interaction $\lambda \boldsymbol{l} \cdot \boldsymbol{s}$.[47,48]

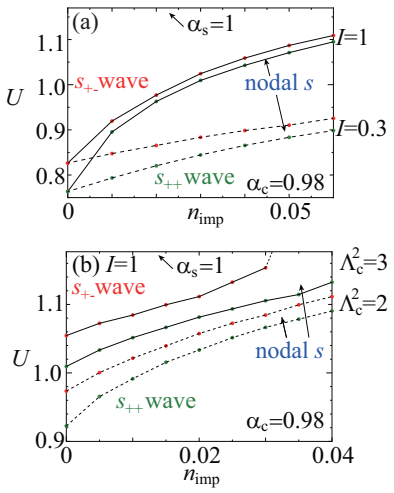

FIG. 10. (Color online) U-$n_{\rm imp}$ phase diagram for $\alpha_c = 0.98$ obtained for (a) $I = 1$ and 0.3 with $\Lambda_c = 1$ and (b) $I = 1$ with $\Lambda_c = \sqrt{2}$ and $\sqrt{3}$.

Moreover, we have recently improve the RPA by including the VC, and found that orbital fluctuations develop strongly in the Hubbard model.[10] Then the orbital susceptibility is $\hat{\chi}^c(q) = [\hat{X}^c(q) + \hat{\chi}^0(q)][1 - \hat{\Gamma}^c[\hat{X}^c(q) + \hat{\chi}^0(q)]]^{-1}$, where $\hat{X}^c(q)$ is the charge VC for the irreducible susceptibility. According to Ref. 10, the magnitude of the three-point vertex is estimated as $\Lambda_c = 1 + X^c(q)/\chi^0(q) \sim 2$, and then Eq. (13) would be replaced by $\hat{V}^c = \frac{1}{2}\Lambda_c^2\hat{\Gamma}^c\hat{\chi}^c\hat{\Gamma}^c$. Figure 10(b) shows the U-$n_{\rm imp}$ phase diagram for $\Lambda_c = \sqrt{2}$ and $\sqrt{3}$, in the case of $I = 1$. We find that the s_{++}-wave region is widely extended, and the nodal-s-wave region is also widened. The gap structure obtained in the crossover regime for $\Lambda_c > 1$ is the loop-shaped nodes shown in Figs. 7–9.

IV. DISCUSSION

In previous sections, we analyzed the gap equations based on a three-dimensional ten-orbital model for $BaFe_2(As,P)_2$. When orbital fluctuations alone are developed, a fully gapped s_{++}-wave state is realized. On the other hand, when spin fluctuations alone are developed, we obtain the $s_{\pm}$-wave state with a horizontal node on a h-FS. During the crossover between s_{++}-wave and $s_{\pm}$-wave states due to the competition between orbital and spin fluctuations, loop-shaped nodes appear on the outer (inner) e-FS when the spin fluctuations are slightly weaker (stronger) than the orbital fluctuations. The phase diagram obtained is shown in Fig. 10. We stress that all three h-FSs are fully gapped during the crossover, since the SC gap on the z^2 orbital originates from the interorbital nesting between different h-FSs.

The crossover from the $s_{\pm}$-wave state to the s_{++}-wave state is also induced by increasing the impurity concentration. In this study, we considered the orbital-diagonal on-site impurity potential at the Fe i site, considering substitution at the Fe site by other elements. In this case, interband impurity scattering is always comparable to intraband scattering, as shown by the T-matrix approximation in Ref. 25. For this reason, when spin fluctuations only are developed, the realized $s_{\pm}$-wave state with $T_{c0} \sim 30$ K is suppressed by small amounts of impurities, with small residual resistivity $\rho_0 \sim 5z^{-1}\ \mu\Omega$ cm ($z^{-1} = m^*/m$ is the mass-enhancement factor). Since $z^{-1} \sim 3$, we can safely expect that the SC state in *dirty Fe-based superconductors* (say, $\rho_0 \sim 100\ \mu\Omega$ cm) would be the s_{++}-wave state due to orbital fluctuations.

There are many important future issues. As we discussed in Sec. III C, one of our important future problems is to study the present 3D ten-orbital Hubbard model ($g = 0$) using the self-consistent VC method developed in Ref. 10. Using this method, we have recently shown that the s_{++}-wave state is realized in the 2D five-orbital Hubbard model ($g = 0$). Note that the ferro orbital fluctuations induced by the VC, which explain the orthorhombic structure transition in Fig. 1, enlarge T_c further.[49] It was recently confirmed that the mechanism of orbital fluctuations due to the VC was realized even in a simple two-orbital model, using the self-consistent VC method as well as the recently developed two-dimensional renormalization group analysis.[43,44]

Another important future issue is to include the self-energy due to orbital and spin fluctuations, Σ^s and Σ^c, into the gap equation. They are given as

$$\hat{\Sigma}^{\xi}(k) = T\sum_{p}(\pm)\hat{V}^{\xi}(p)\hat{G}(k+p), \tag{24}$$

where the positive (negative) sign corresponds to $\xi = c$ ($\xi = s$). The real and imaginary parts of the total self-energy $\hat{\Sigma}(k) = \hat{\Sigma}^c(k) + \hat{\Sigma}^s(k)$ represent the mass enhancement and quasiparticle inelastic scattering, respectively. Both effects suppress T_c. Moreover, the orbital and momentum dependence of $\hat{\Sigma}(k)$ would strongly modify the anisotropy of the SC gap functions. Thus, the self-energy correction in the gap equation will be important for the quantitative analysis of the SC gaps.

V. SUMMARY

In this paper, we studied the SC gap structure using a ten-orbital model for $BaFe_2(As,P)_2$. When the orbital fluctuations due to the interorbital quadrupole interaction (3) are strong, the s_{++}-wave state is realized. In contrast, the $s_{\pm}$-wave state is formed by strong spin fluctuations, mainly due to the intraorbital Coulomb interaction U. Both spin and orbital fluctuations will develop strongly in the optimally doped regime near the O phase. In this case, we find that a smooth crossover between the s_{++}- and $s_{\pm}$-wave states is realized by changing the interactions or the impurity concentration, without a large suppression in T_c.

During this $s_{++} \leftrightarrow s_{\pm}$ crossover, the loop-shaped nodes are universally formed on the e-FSs, as a result of the competition between interorbital attractive and intraorbital repulsive interactions. This result is consistent with recent angle-resolved thermal conductivity[34] and ARPES measurements.[33] During the crossover, the SC gaps on the h-FSs are fully gapped and almost orbital independent due to the orbital fluctuations, consistently with recent ARPES measurements.[32,33]

ACKNOWLEDGMENTS

We are grateful to Y. Matsuda, T. Shibauchi, A. Fujimori, T. Yoshida, S. Shin, T. Shimojima, D. S. Hirashima, and Y. Yamakawa for valuable discussions. This study has been supported by Grants-in-Aid for Scientific Research from MEXT of Japan. Numerical calculations were partially performed using the Yukawa Institute Computer Facility.

APPENDIX A: ORBITAL SUSCEPTIBILITIES IN THE PRESENT MODEL

In this paper, we discussed the development of orbital fluctuations due to the quadrupole interaction in Eq. (3). Here, we consider the quadrupole operator at $i = (a,\alpha)$, where a and α represent the unit cell and the Fe site (A or B), respectively. Then the operator $\hat{O}^i_{\Gamma}$ ($\Gamma = xz, yz, xy$) is given as

$$\hat{O}^i_{\Gamma} \equiv \sum_{lm} o^{l,m}_{\Gamma}\hat{m}^i_{l,m}, \tag{A1}$$

where l and m represents the d orbital, $\hat{m}^i_{l,m} \equiv \sum_{\sigma} c^{\dagger}_{li\sigma}c_{mi\sigma}$, and the coefficient is defined as $o^{l,m}_{xz} = 7\langle l|\hat{x}\hat{z}|m\rangle$ for $\Gamma = xz$, where $\hat{x} = x/r$ and so on. The nonzero coefficients are given

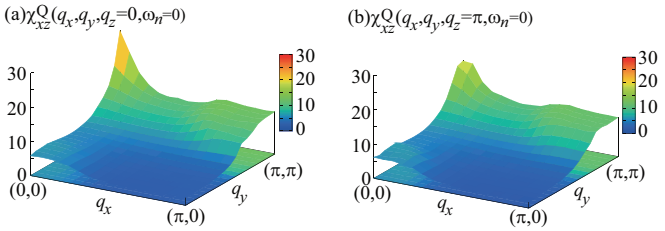

FIG. 11. (Color online) O_{xz}-channel quadrupole fluctuations $\chi^Q_{xz}(\boldsymbol{q},0)$ obtained for $n = 6.0$ and $\alpha_c = 0.98$, in the (a) $q_z = 0$ plane and (b) $q_z = \pi$ plane. The obtained q_z dependence of $\chi^Q_{xz}(\boldsymbol{q},0)$ is rather weak.

as[41]

$$o^{2,5}_{xz} = o^{3,4}_{xz} = \sqrt{3}o^{1,2}_{xz} = 1, \tag{A2}$$

$$-o^{3,5}_{yz} = o^{2,4}_{yz} = \sqrt{3}o^{1,3}_{yz} = 1, \tag{A3}$$

$$o^{2,3}_{xy} = -\sqrt{3}o^{1,4}_{xy}/2 = 1, \tag{A4}$$

where 1,2,3,4,5 respectively correspond to z^2, xz, yz, xy, $x^2 - y^2$.

In the presence of quadrupole interaction in Eq. (3), $\hat{\chi}^c(q)$ given in Eq. (6) is strongly enhanced. Then it is convenient to introduce the quadrupole interaction, by $\hat{\chi}^{Q,\alpha\beta}_{\Gamma}(q) \equiv \hat{o}_\Gamma \hat{\chi}^{c,\alpha\beta}(q)\hat{o}_\Gamma\}$, where $\alpha,\beta = A$ or B. In the present study, the channel $\Gamma = xz,yz$ is the most strongly enhanced, due to the good interorbital nesting in Fe-based superconductors.[19] Figure 11 shows the obtained $\hat{\chi}^Q_{xz}(\boldsymbol{q},0) = \hat{\chi}^{Q,AA}_{xz}(\boldsymbol{q},0) + \hat{\chi}^{Q,AB}_{xz}(\boldsymbol{q},0)$ in the $q_z = 0$ and $q_z = \pi$ planes.[41] The large peak at $\boldsymbol{q} \approx (0,\pi)$ originates from the interorbital $(yz \leftrightarrow xy)$ nesting between the e-FS and h-FS, and the small peak at $\boldsymbol{q} \approx (\pi,\pi)$ originates from the interorbital $(xz \leftrightarrow z^2)$ nesting between two h-FSs. Therefore, the development obtained for $\hat{\chi}^Q_{xz}(q)$ and $\hat{\chi}^Q_{yz}(q)$ means the existence of strong orbital fluctuaitions on the xz, yz, xy, and z^2 orbitals, of which the FSs of $BaFe_2(As,P)_2$ are composed. For this reason, we obtain the orbital-fluctuation-mediated s_{++}-wave state with an approximately isotropic SC gap on the three h-FSs, consistently with the ARPES measurements in Refs. 32 and 33.

In addition to the antiferro (AF) orbital fluctuation, the ferro orbital fluctuations with respect to $O_{x^2-y^2} = n_{xz} - n_{yz}$ are induced by the "two-orbiton process" in Ref. 41 as well as the "two-magnon process" in Ref. 10. These processes are given by the Azlamasov-Larkin (AL) type of vertex correction, since the AL term describes the interference between ferro and AF fluctuations that is neglected in the RPA. The ferro orbital fluctuations induce the softening of C_{66} as well as the orthorhombic structure transition. Although the ferro orbital fluctuations also contribute to the s-wave SC state, we consider that they are not the major mechanism of the SC: First, the relation $\Delta_{xz},\Delta_{yz} \gg \Delta_{xy}$ is expected in the ferro-orbital-fluctuation-mediated s_{++}-wave state, since these fluctuations develop only on the xz and yz orbitals. This relation is inconsistent with experiments. Second, we have recently solved the Eliashberg gap equation based on the self-consistent VC method[49] and found that the main pairing interaction actually comes from AF orbital fluctuations with respect to

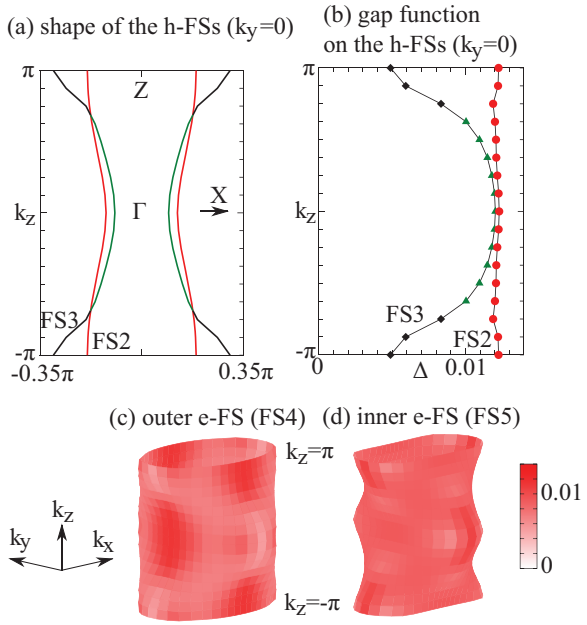

FIG. 12. (Color online) SC gap functions obtained in the overdoped case ($n = 6.1$) for $g = 0.25$, $U = 0$, and $n_{\rm imp} = 0$. (a) k_z dependence of the h-FSs, and (b) the SC gap functions obtained on the h-FSs. We also show the 3D gap functions on the (c) outer and (d) inner e-FS.

$O_{xz,yz}$, since the peak of the ferro orbital susceptibility is very narrow in the momentum space. Therefore, the present analysis taking only AF orbital fluctuations seems to be justified.

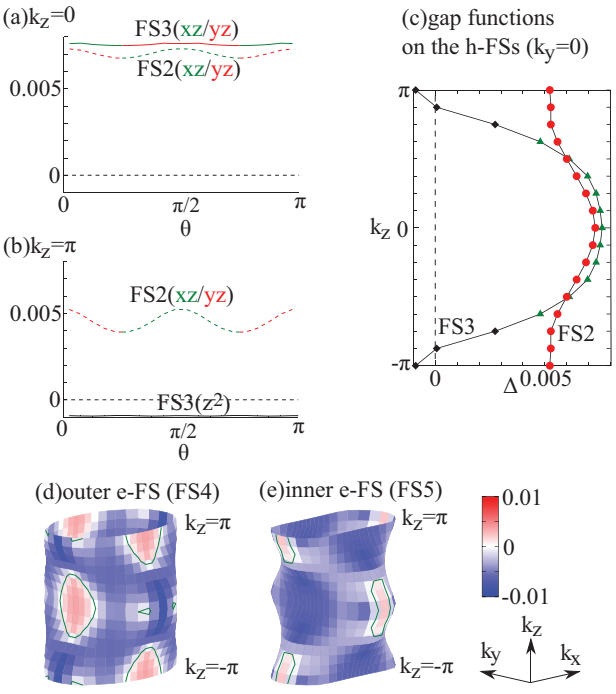

FIG. 13. (Color online) SC gap functions obtained in the overdoped case ($n = 6.1$) for $g = 0$, $U = 1.37$, and $n_{\rm imp} = 0$. (a), (b) SC gap functions on the h-FSs in the $k_z = 0$ and $k_z = \pi$ planes. (c) k_z dependence of SC gap functions on the h-FSs for $k_y = 0$. (d), (e) 3D gap functions on the outer and inner e-FS, respectively.

APPENDIX B: HEAVILY ELECTRON-DOPED CASE

In this paper, we have studied the gap functions for $n = 6.0$. In this Appendix, we discuss the heavily electron-doped case ($n = 6.1$). Figure 12(a) shows the h-FSs on the $k_y = 0$ plane. As one can see, the xy-orbital h-FS disappears.

Now, we consider the orbital-fluctuation-mediated s_{++}-wave SC state. Here, we put $g = 0.25$ ($\alpha_c = 0.98$) and $U = 0$ and the eigenvalue λ_E obtained is 0.87. First, we discuss the SC gaps on the h-FSs. Figure 12(b) shows the k_z dependence of the SC gaps on the h-FSs in the $k_y = 0$ plane. In contrast to the case of $n = 6.0$, the SC gap on the z^2-orbital hole FS becomes smaller, while each SC gap on the h-FSs on any plane perpendicular to the k_z axis is almost isotropic. Next, we focus on the SC gaps on the e-FSs. Figures 12(c) and 12(d) show the 3D gap functions on the outer and inner e-FSs, respectively. As with the case of $n = 6.0$, the SC gaps on the e-FSs are nearly isotropic on any plane perpendicular to the k_z axis.

Next, we discuss the spin-fluctuation-mediated $s_{\pm}$-wave SC state. Here, we put $U = 1.37$ ($\alpha_s = 0.98$) and $g = 0$. The eigenvalue λ_E obtained is 1.68. Figures 13(a) and 13(b) show the gap functions on the h-FSs in the $k_z = 0$ and $k_z = \pi$ planes, respectively. In common with the results for $n = 6.0$, the SC gap function on the z^2-orbital h-FS is almost zero since the spin fluctuations in the z^2 orbital do not develop. Figure 13(c) shows the k_z dependence on the SC gaps on the h-FSs in the $k_y = 0$ plane. It clearly shows the horizontal line node on FS3 near $k_z = \pi$.

Next, we discuss the e-FSs. Figures 13(d) and 13(e) show the 3D gap functions on the outer and inner e-FSs, respectively. Unlike in the case of $n = 6.0$, line nodes appear on the e-FSs even when $g = 0$. This result is consistent with the analysis in Ref. 31: a nodal gap appears on the e-FSs when the xy-orbital h-FS disappears because of the competition of different spin fluctuations; $\boldsymbol{Q} = (\pi,0)$ on the $xz + yz$ orbitals and $\boldsymbol{Q} = (\pi,\pi/2)$ on the xy orbital. In the presence of the xy-orbital h-FS for $n \approx 6.0$, on the other hand, spin fluctuations develop at $\boldsymbol{Q} = (\pi,0)$ in all d orbitals. Then a fully gapped $s_{\pm}$-wave state is realized. In this case, the competition of orbital and spin fluctuations induces the loop-shaped nodes discussed in Sec. III C.

We comment that Khodas and Chubukov discussed the emergence of the loop-shaped nodes on e-FSs in the "folded model" with two Fe atoms in each unit cell:[50] When "vertical nodes" of e-FSs are realized in the "unfolded model" with one Fe atom in each unit cell, loop-shaped nodes are realized in the folded model by taking the finite hybridization between two e-FSs inherent in 122 systems[40] into account. Within the RPA, the vertical nodes appear only in the absence of an xy-like hole pocket at (π,π) as discussed by Kuroki *et al.*,[31] and therefore the mechanism of formation of the loop-shaped nodes by Khodas and Chubukov requires the absence of xy-like hole pockets, at least within the RPA. The calculation in this appendix gives a numerical verification of the theory of Khodas and Chubukov.

[1] Y. Kamihara, T. Watanabe, M. Hirano, and H. Hosono, J. Am. Chem. Soc. **130**, 3296 (2008).

[2] M. Yi, D. H. Lu, J.-H. Chu, J. G. Analytis, A. P. Sorini, A. F. Kemper, S.-K. Mo, R. G. Moore, M. Hashimoto, W. S. Lee, Z. Hussain, T. P. Devereaux, I. R. Fisher, and Z.-X. Shen, Proc. Natl. Acad. Sci. USA **108**, 6878 (2011).

[3] R. M. Fernandes, L. H. VanBebber, S. Bhattacharya, P. Chandra, V. Keppens, D. Mandrus, M. A. McGuire, B. C. Sales, A. S. Sefat, and J. Schmalian, Phys. Rev. Lett. **105**, 157003 (2010).

[4] M. Yoshizawa, R. Kamiya, R. Onodera, Y. Nakanishi, K. Kihou, H. Eisaki, and C. H. Lee, J. Phys. Soc. Jpn. **81**, 024604 (2012).

[5] T. Goto, R. Kurihara, K. Araki, K. Mitsumoto, M. Akatsu, Y. Nemoto, S. Tatematsu, and M. Sato, J. Phys. Soc. Jpn. **80**, 073702 (2011).

[6] J. L. Niedziela, D. Parshall, K. A. Lokshin, A. S. Sefat, A. Alatas, and T. Egami, Phys. Rev. B **84**, 224305 (2011).

[7] F. Kruger, S. Kumar, J. Zaanen, and J. van den Brink, Phys. Rev. B **79**, 054504 (2009).

[8] W. Lv, J. Wu, and P. Phillips, Phys. Rev. B **80**, 224506 (2009).

[9] C. C. Lee, W.-G. Yin, and W. Ku, Phys. Rev. Lett. **103**, 267001 (2009).

[10] S. Onari and H. Kontani, Phys. Rev. Lett. **109**, 137001 (2012).

[11] I. R. Fisher, L. Degiorgi, and Z. X. Shen, Rep. Prog. Phys. **74**, 124506 (2011).

[12] S. Kasahara, H. J. Shi, K. Hashimoto, S. Tonegawa, Y. Mizukami, T. Shibauchi, K. Sugimoto, T. Fukuda, T. Terashima, Andriy H. Nevidomskyy, and Y. Matsuda, Nature (London) **486**, 382 (2012).

[13] S. Ishida, M. Nakajima, T. Liang, K. Kihou, C. H. Lee, A. Iyo, H. Eisaki, T. Kakeshita, Y. Tomioka, T. Ito, and S. Uchida, Phys. Rev. Lett. **110**, 207001 (2013).

[14] Y. Inoue, Y. Yamakawa, and H. Kontani, Phys. Rev. B **85**, 224506 (2012).

[15] K. Kuroki, S. Onari, R. Arita, H. Usui, Y. Tanaka, H. Kontani, and H. Aoki, Phys. Rev. Lett. **101**, 087004 (2008).

[16] I. I. Mazin, D. J. Singh, M. D. Johannes, and M. H. Du, Phys. Rev. Lett. **101**, 057003 (2008).

[17] S. Graser, G. R. Boyd, C. Cao, H.-P. Cheng, P. J. Hirschfeld, and D. J. Scalapino, Phys. Rev. B **77**, 180514(R) (2008).

[18] A. V. Chubukov, D. V. Efremov, and I. Eremin, Phys. Rev. B **78**, 134512 (2008).

[19] H. Kontani and S. Onari, Phys. Rev. Lett. **104**, 157001 (2010).

[20] T. Saito, S. Onari, and H. Kontani, Phys. Rev. B **82**, 144510 (2010).

[21] A. Kawabata, S. C. Lee, T. Moyoshi, Y. Kobayashi, and M. Sato, J. Phys. Soc. Jpn. **77**, 103704 (2008); M. Sato, Y. Kobayashi, S. C. Lee, H. Takahashi, E. Satomi, and Y. Miura, *ibid.* **79**, 014710 (2009); S. C. Lee, E. Satomi, Y. Kobayashi, and M. Sato, *ibid.* **79**, 023702 (2010).

[22] Y. Nakajima, T. Taen, Y. Tsuchiya, T. Tamegai, H. Kitamura, and T. Murakami, Phys. Rev. B **82**, 220504 (2010).

[23] J. Li, Y. Guo, S. Zhang, S. Yu, Y. Tsujimoto, H. Kontani, K. Yamaura, and E. Takayama-Muromachi, Phys. Rev. B **84**, 020513(R) (2011).

[24] K. Kirshenbaum, S. R. Saha, S. Ziemak, T. Drye, and J. Paglione, Phys. Rev. B **86**, 140505 (2012).

[25]S. Onari and H. Kontani, Phys. Rev. Lett. **103**, 177001 (2009); Y. Yamakawa, S. Onari, and H. Kontani, Phys. Rev. B **87**, 195121 (2013).
[26]S. Onari, H. Kontani, and M. Sato, Phys. Rev. B **81**, 060504(R) (2010); S. Onari and H. Kontani, *ibid.* **84**, 144518 (2011).
[27]M. A. Tanatar, J.-Ph. Reid, H. Shakeripour, X. G. Luo, N. Doiron-Leyraud, N. Ni, S. L. Budko, P. C. Canfield, R. Prozorov, and L. Taillefer, Phys. Rev. Lett. **104**, 067002 (2010).
[28]H. Kontani, Phys. Rev. B **70**, 054507 (2004).
[29]S. Graser, A. F. Kemper, T. A. Maier, H.-P. Cheng, P. J. Hirschfeld, and D. J. Scalapino, New J. Phys. **12**, 073030 (2010); Phys. Rev. B **81**, 214503 (2010).
[30]S. Maiti, M. M. Korshunov, T. A. Maier, P. J. Hirschfeld, and A. V. Chubukov, Phys. Rev. Lett. **107**, 147002 (2011); Phys. Rev. B **84**, 224505 (2011).
[31]K. Kuroki, H. Usui, S. Onari, R. Arita, and H. Aoki, Phys. Rev. B **79**, 224511 (2009).
[32]T. Shimojima *et al.*, Science **332**, 564 (2011).
[33]T. Yoshida *et al.*, arXiv:1301.4818.
[34]M. Yamashita, Y. Senshu, T. Shibauchi, S. Kasahara, K. Hashimoto, D. Watanabe, H. Ikeda, T. Terashima, I. Vekhter, A. B. Vorontsov, and Y. Matsuda, Phys. Rev. B **84**, 060507(R) (2011).
[35]Y. Zhang, Z. R. Ye, Q. Q. Ge, F. Chen, Juan Jiang, M. Xu, B. P. Xie, and D. L. Feng, Nat. Phys. **8**, 371 (2012).
[36]K. Suzuki, H. Usui, and K. Kuroki, J. Phys. Soc. Jpn. **80**, 013710 (2011).
[37]J. S. Kim, P. J. Hirschfeld, G. R. Stewart, S. Kasahara, T. Shibauchi, T. Terashima, and Y. Matsuda, Phys. Rev. B **81**, 214507 (2010).
[38]Y. Wang, J. S. Kim, G. R. Stewart, P. J. Hirschfeld, S. Graser, S. Kasahara, T. Terashima, Y. Matsuda, T. Shibauchi, and I. Vekhter, Phys. Rev. B **84**, 184524 (2011).
[39]D. V. Efremov, M. M. Korshunov, O. V. Dolgov, A. A. Golubov, and P. J. Hirschfeld, Phys. Rev. B **84**, 180512(R) (2011).
[40]T. Saito, S. Onari, and H. Kontani, Phys. Rev. B **83**, 140512(R) (2011).
[41]H. Kontani, T. Saito, and S. Onari, Phys. Rev. B **84**, 024528 (2011).
[42]H. Kontani, Y. Inoue, T. Saito, Y. Yamakawa, and S. Onari, Solid State Commun. **152**, 718 (2012).
[43]Y. Ohno, M. Tsuchiizu, S. Onari, and H. Kontani, J. Phys. Soc. Jpn. **82**, 013707 (2013).
[44]M. Tsuchiizu, S. Onari, and H. Kontani, arXiv:1209.3664.
[45]J. Kunes, R. Arita, P. Wissgott, A. Toschu, H. Ikeda, and K. Held, Comput. Phys. Commun. **181**, 1888 (2010).
[46]T. Takimoto, T. Hotta, T. Maehira, and K. Ueda, J. Phys.: Condens. Matter **14**, L369 (2002).
[47]Paul Steffens, C. H. Lee, N. Qureshi, K. Kihou, A. Iyo, H. Eisaki, and M. Braden, arXiv:1210.6386.
[48]O. J. Lipscombe, L. W. Harriger, P. G. Freeman, M. Enderle, C. Zhang, M. Wang, T. Egami, J. Hu, T. Xiang, M. R. Norman, and P. Dai, Phys. Rev. B **82**, 064515 (2010).
[49]S. Onari and H. Kontani (unpublished).
[50]M. Khodas and A. V. Chubukov, Phys. Rev. B **86**, 144519 (2012).